Nanotechnology

PAPER

Stress evolution of Ge nanocrystals in dielectric matrices

To cite this article: Rahim Bahariqushchi *et al* 2018 *Nanotechnology* **29** 185704

View the article online for updates and enhancements.

Related content

- Nanocrystals for silicon-based light-emitting and memory devices
  S K Ray, S Maikap, W Banerjee et al.
- Characterization of Ge nanocrystals embedded in SiO2 by Raman spectroscopy
  U Serincan, G Kartopu, A Guennes et al.
- Influence of reductant and germanium concentration on the growth and stress developmentof germanium nanocrystals in silicon oxide matrix
  H G Chew, F Zheng, W K Choi et al.

IOP ebooks™

Bringing you innovative digital publishing with leading voices to create your essential collection of books in STEM research.

Start exploring the collection - download the first chapter of every title for free.

This content was downloaded from IP address 139.179.72.242 on 25/02/2019 at 05:50

IOP Publishing

Nanotechnology

Nanotechnology 29 (2018) 185704 (14pp)

https://doi.org/10.1088/1361-6528/aaaffa

Stress evolution of Ge nanocrystals in dielectric matrices

Rahim Bahariqushchi[1], Rosario Raciti[2], Ahmet Emre Kasapoğlu[3], Emre Gür[3,4], Meltem Sezen[5], Eren Kalay[6], Salvatore Mirabella[2] and A Aydinli[7,8,9]

[1] Bilkent University, Physics Department, Ankara, Turkey
[2] MATIS CNR-IMM and University of Catania, Department of Physics and Astronomy, Catania, Italy
[3] East Anatolia High Technology Application and Research Center, Turkey
[4] Atatürk University, Department of Physics, 25240, Erzurum, Turkey
[5] Sabancı University, SUNUM, Istanbul, Turkey
[6] Middle East Technical University, Department of Material Science, Ankara, Turkey
[7] Uludag University, Electrical and Electronics Engineering Department, Bursa, Turkey

E-mail: aydinli@fen.bilkent.edu.tr

Received 7 November 2017, revised 29 January 2018
Accepted for publication 16 February 2018
Published 8 March 2018

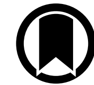

Abstract

Germanium nanocrystals (Ge NCs) embedded in single and multilayer silicon oxide and silicon nitride matrices have been synthesized using plasma enhanced chemical vapor deposition followed by conventional furnace annealing or rapid thermal processing in N_2 ambient. Compositions of the films were determined by Rutherford backscattering spectrometry and x-ray photoelectron spectroscopy. The formation of NCs under suitable process conditions was observed with high resolution transmission electron microscope micrographs and Raman spectroscopy. Stress measurements were done using Raman shifts of the Ge optical phonon line at 300.7 cm^{-1}. The effect of the embedding matrix and annealing methods on Ge NC formation were investigated. In addition to Ge NCs in single layer samples, the stress on Ge NCs in multilayer samples was also analyzed. Multilayers of Ge NCs in a silicon nitride matrix separated by dielectric buffer layers to control the size and density of NCs were fabricated. Multilayers consisted of SiN_y:Ge ultrathin films sandwiched between either SiO_2 or Si_3N_4 by the proper choice of buffer material. We demonstrated that it is possible to tune the stress state of Ge NCs from compressive to tensile, a desirable property for optoelectronic applications. We also observed that there is a correlation between the stress and the crystallization threshold in which the compressive stress enhances the crystallization, while the tensile stress suppresses the process.

Keywords: germanium nanostructures, superlattices, Raman spectroscopy, stress tuning, transmission electron microscopy, dielectric matrices

(Some figures may appear in colour only in the online journal)

Introduction

Silicon and germanium nanocrystals (Ge NCs) embedded in wide band gap dielectric materials such as SiO_2, Si_3N_4 and Al_2O_3 have attracted a lot of attention in the past decade due to their potential applications in third generation solar cells [1], highly efficient quantum dot photodetectors [2], optoelectronics [3] and nonvolatile memory devices [4]. Si is the preferred material due to its abundance in nature and nontoxicity. However, Ge has its advantages over Si due to its larger Bohr radius (24.3 nm) [5] when compared with Si (4.9 nm), which leads to a stronger quantum confinement effect at the same size as well as easier tuning of the band gap [6]. Furthermore, Ge has a lower melting point (938 °C) compared to Si (1414 °C), which leads to much

[8] Formerly at Bilkent University, Physics Department, Ankara, 06800, Turkey.
[9] Author to whom any correspondence should be addressed.

 © 2018 IOP Publishing Ltd Printed in the UK

lower processing temperatures and, therefore, reduced thermal budget. Most of the works focus on Ge NCs embedded in oxide matrices like SiO_2 and Al_2O_3 [7–9]. However, oxidation of Ge NCs embedded in oxide matrices is an important issue [10, 11] that gives rise to a high barrier height for the NCs in the oxide matrix hindering carrier transport [11]. Fabrication of Ge NCs in a silicon nitride matrix might be a solution for these problems.

One of the main issues in the synthesis of NCs in dielectric matrices is the associated resident stress on the NCs [12]. The origin of this stress is usually attributed to mismatch between NC and matrix lattice constants and the difference in coefficients of thermal expansion. In the case of Ge nanocrystals, expansion upon solidification of liquid Ge droplets is suggested to be the source of compressive stress [12]. Moreover, strain can modify the structural and optical properties of solids. Yuan *et al* [13] studied the structural phase transitions of Si nanocrystals induced by strain in pulsed laser deposited and rapid thermal annealed amorphous Al_2O_3 matrices. They found that microstructure and photoluminescence are closely related to the amount of strain. Even in rare earth oxide matrices, phase transitions as well as the enhanced crystal growth of ternary compound NCs have been observed [14]. Both compressive and tensile stress on Ge nanodots and NCs have been observed in samples fabricated with a complementary metal-oxide-semiconductor-compatible process within SiO_2 and Si_3N_4 layers [15]. Compressive stress as high as 4.5% and tensile stress as high as 1.0% have been observed in Si_3N_4 and SiO_2 matrices, respectively, each of which were explained by different mechanisms. Stressors such as silicon nitride have been used to induce strain in Ge waveguides used in Ge lasers [16].

Several techniques have been proposed to apply tensile stress to Ge NCs. One way is to use the difference between thermal expansion coefficients between Ge and Si that can lead to 0.25% tensile strain [17]. Another way is to use buffer layers like InGaAs [18], germanium tin [19] and Si_3N_4 [20]. Si_3N_4 is a material that is widely used as a stressor in the microelectronics industry. There are reports that show the potential of exploiting Si_3N_4 in photonic applications by creating tensile strain in germanium nanostructures [20].

In this work, we study the effect of the surrounding dielectric matrix on Ge NCs. Single layers of SiO_2 and Si_3N_4 with Ge NCs as well as multilayers were studied. Multilayers were ultrathin Ge nanocrystals embedded in a silicon nitride matrix and buffered by either SiO_2 or Si_3N_4 synthesized by the plasma enhanced chemical vapor deposition (PECVD) technique. We show the evolution of stress from compressive to tensile by suitable buffer material selection and the effect of stress on crystallization.

Experimental

Ge NCs embedded in dielectric matrices were fabricated in a PECVD reactor (PlasmaLab 8510C) and post annealing. Four sets of samples were fabricated: the first set was composed of single layer SiN_y:Ge thin films with thickness around 200 nm where we varied the composition of the layers to determine the optimum Ge concentration. The second set was single layers of SiO_y:Ge thin films with thickness around 200 nm. The third set was superlattices consisting of eight bilayers of SiN_y:Ge/SiO_2. In this set, SiN_y:Ge films had thicknesses varying between 3.0 and 9.0 nm, and SiO_2 was stoichiometric silicon oxide, which performed as a buffer layer for diffusion of Ge atoms during the annealing process and, therefore, controlling the size of the NCs. The thickness of SiO_2 layers for all samples was around 25 nm. The fourth set consisted of superlattices with eight bilayers of SiN_y:Ge/Si_3N_4. This set was similar to the third set with Si_3N_4 being the buffer layer. A schematic of the four sets of samples is shown in figure 1. For growing SiN_y:Ge thin films a mixture of SiH_4, NH_3 and GeH_4 gases was used as process gases. The compositions of as-prepared samples were analyzed via Rutherford backscattering spectrometry (RBS) and/or x-ray photoelectron spectroscopy (XPS) techniques. RBS measurements were carried out with a 3.5 MeV HVEE Singletron accelerator, using a 2.0 MeV He^+ beam in random configuration and with a backscattered angle of 165°. RBS spectra were simulated using SIMNRA software to determine the Si, Ge, and N content and the stoichiometry of each film [21]. XPS measurements were done by using a Specs Flex-Mod system. Monochromatized AlKα x-rays were used for the measurements. A flood gun with low energy was used to neutralize the charging. For most samples, annealing was done in a cylindrical conventional furnace up to 900° C for 30 min or more. To investigate the role of the annealing method, some samples were also processed via rapid thermal processing (RTP). Raman spectroscopy was performed using 514.5 wavelength of Ar ion laser. Electron microscopy was done via a 300 KV TECNAI f30 field emission transmission electron microscope (TEM). TEM specimens were prepared using a JEOL JIB 4601F MultiBeam FIB-SEM platform using Ga^+ ions for obtaining ultrathin and homogeneous cross-sectional lamellae from the corresponding samples. For the TEM sample preparation the lift-out technique was used in the FIB, in which two trenches were milled away on the samples with relatively high ion currents (5–30 nA) and the middle section was carried to a TEM grid. This stage was then followed by polishing the section by applying lower ion currents (10–100 pA) until an electron-transparent thickness on the lamella was achieved. TEM sample preparation using the FIB lift-out technique is shown in figure 2.

Results and discussion

Stress on Ge nanocrystals in single layer dielectrics

The most critical parameter affecting the formation of nanocrystals in dielectric matrices is the amount of Ge in the thin film and its composition before formation of the NCs by annealing.

Ge content is a determining parameter in controlling the size and density of nanocrystals [22].

Several techniques were applied to determine the composition of the dielectric thin films. We, first applied RBS as Ge is a heavy atom and easily observed during backscattering

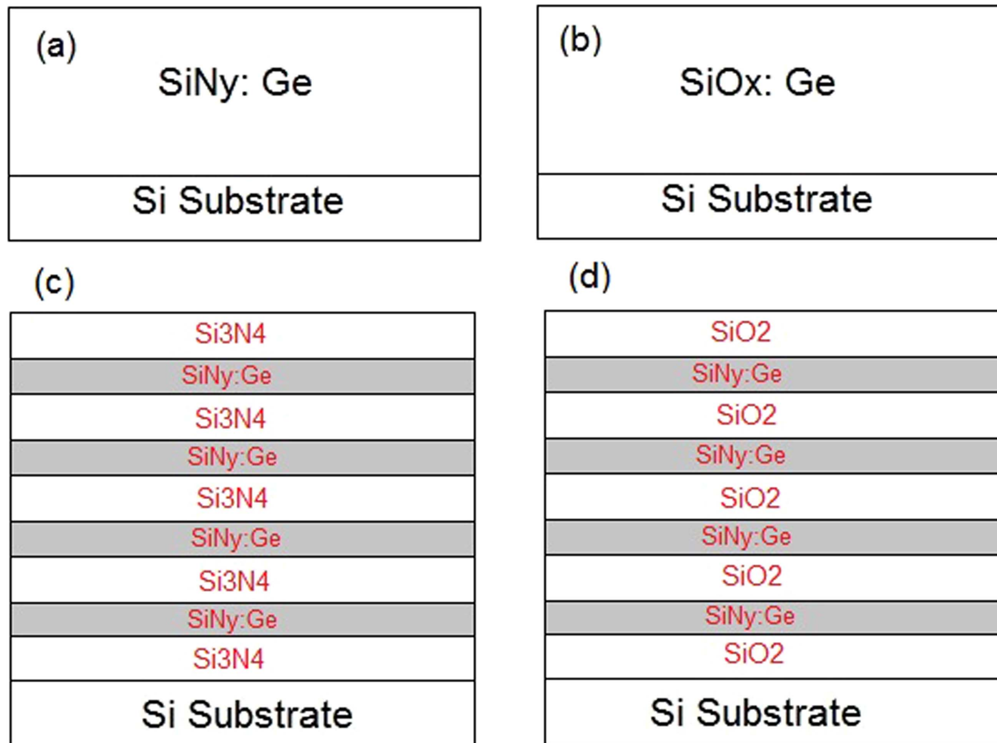

Figure 1. Schematic diagram of four set of samples. (a) and (b) Ge NCs embedded in silicon nitride and silicon oxide matrices, respectively. (c) and (d) Multilayers consisting of Ge NCs in a silicon nitride matrix separated by Si_3N_4 and SiO_2 thin films, respectively.

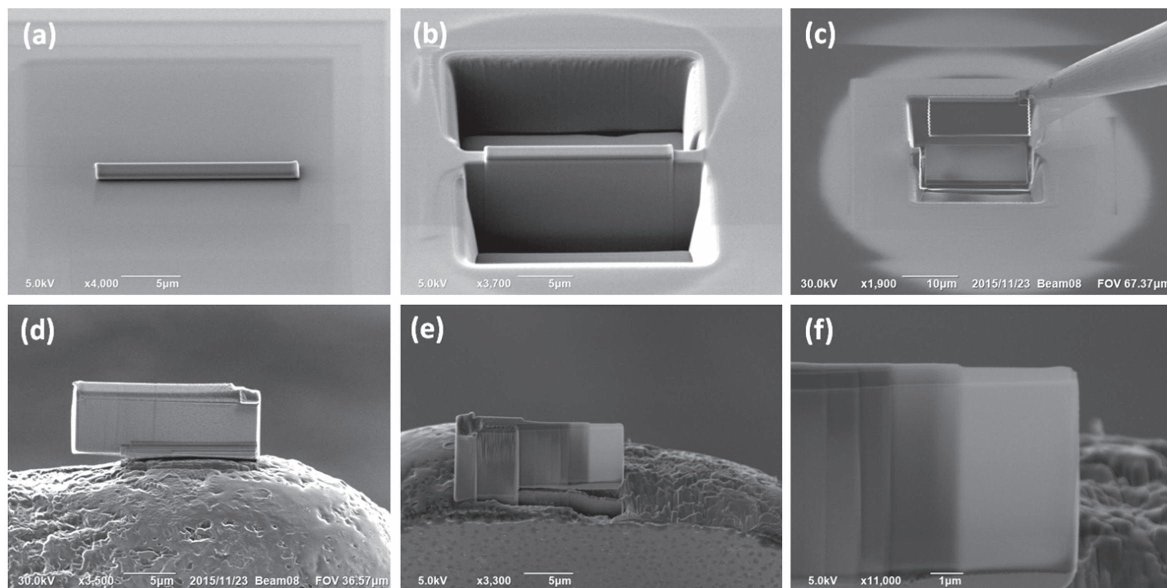

Figure 2. TEM sample preparation using focused ion beams. (a) A protective carbon layer is deposited on the region of interest. (b) Trenches are ion milled. (c) The pre-section is lifted out with the help of a micromanipulator. (d) A cross-section is mounted on the TEM grid. (e) The sample is ion-polished. (f) The electron-transparent (<100 nm) thickness is reached.

of He ions. A representative analysis performed using RBS can be seen in figure 3, which shows the RBS spectra of SiN_y:Ge films deposited on a silicon substrate.

Arrows indicate the signals due to Ge, Si and N in the SiN_y:Ge film (starting respectively at around 1600, 1150 and 630 keV of the He^+ backscattered energy for the used configuration). All samples exhibit a homogeneous depth distribution of Ge atoms and the spectra were fitted through SIMNRA software simulation, figure 3(b), in order to estimate the atomic content of Si, Ge and N in the film. Table 1 summarizes the ratios of Ge/Si and Ge/N evaluated by RBS analysis for SiN_y:Ge films. The Ge content in SiN_y:Ge films increases with the GeH_4 flux, from 4% to about 24%. Ge dose were found to be 45, 95, 190 and 275 $\times$ 10^{15} at cm^{-2},

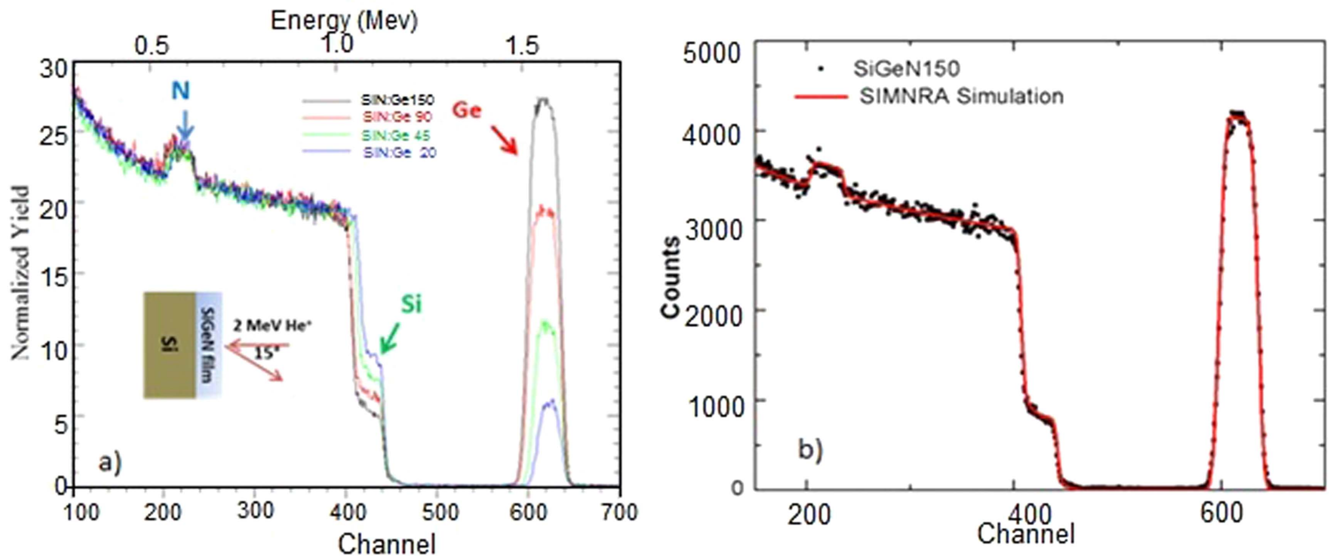

Figure 3. (a) RBS spectra of SiN_y:Ge thin films. The backscattered signal due to Ge is obvious with Si and N displaying significant shoulders. The inset image represents the schematic of the experimental setup. (b) SIMNRA simulation of the RBS spectra to determine the composition.

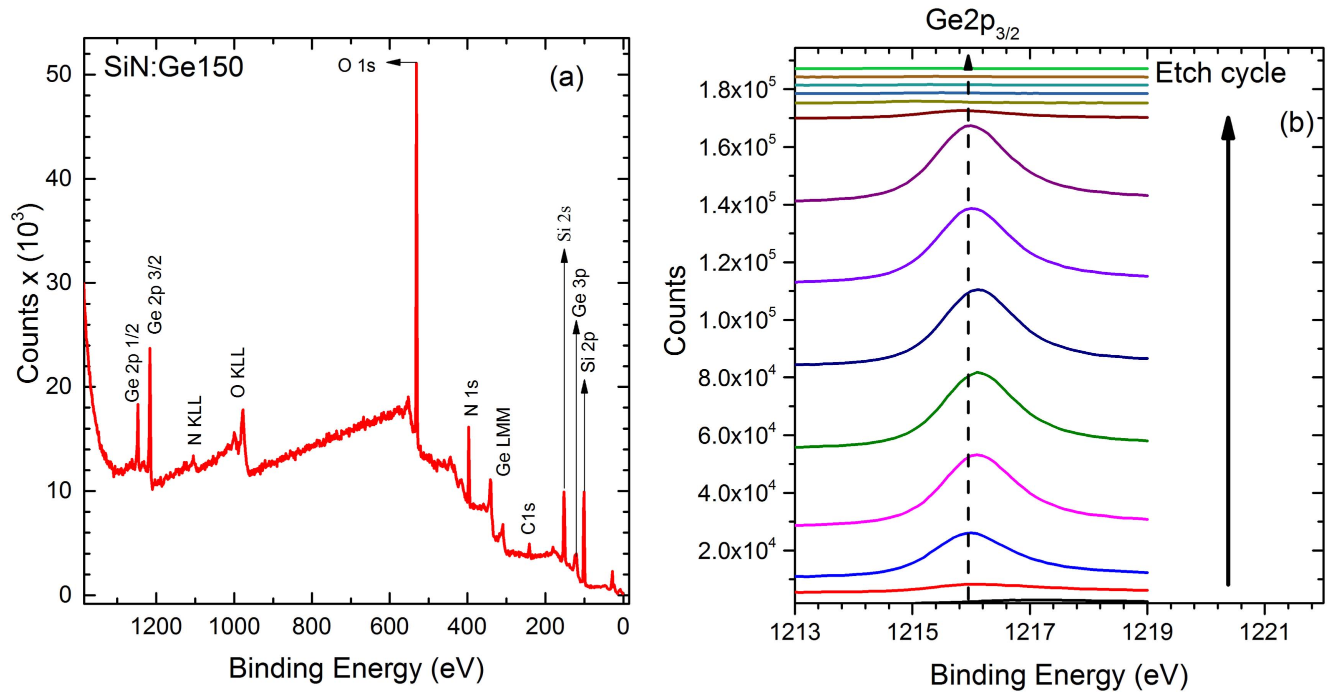

Figure 4. XPS measurements of the SiN:Ge150 sample. (a) Survey spectrum. (b) Depth profile of the Ge $2p_{3/2}$ line.

Table 1. Sample description and properties of SiN_y:Ge thin films with various concentrations of Ge. Atomic doses are determined in terms of atoms cm^{-2} which can be converted into mole fractions once the densities are known. Relative error is ~5%.

Sample ID	GeH_4 (sccm)	Ge dose (E15 at cm^{-2})	Ge/Si/N ratio	% Ge
SiN:Ge 20	20	45	1/7.5/9.5	4
SiN:Ge 45	45	95	1/3.5/5	9
SiN:Ge 90	90	190	1/1.5/2.5	15
SiN:Ge150	150	275	1/1/1.5	24

respectively. Buffer layers were similarly analyzed and were determined to be stoichiometric under the growth conditions used in this study. The results are summarized in table 1.

The second technique used to find the Ge percentage was XPS. In addition, depth profile XPS measurements were used to find out the chemical environment of the Ge NCs. A representative XPS survey spectrum and depth profile measurements on the single layer SiN:Ge150 are shown in figure 4.

Figure 4(a) shows the survey spectrum of the sample investigated. Only peaks belonging to the elements of Si, Ge, N, O and C were observed, as shown in the figure. Observed C and O elements are due to surface contamination. Adventitious C 1s energy was used to correct the spectrum. Depth profile XPS measurements were used to determine the chemical state of Ge. Figure 4(b) shows the Ge $2p_{3/2}$ lines after every etch cycle. No significant change in the binding energy of the Ge $2p_{3/2}$ line was observed. This shows that the Ge NCs are in the same chemical environment in the Si_3N_4 matrices throughout the thickness of Ge NC containing layers.

The most direct approach to structural analysis of such samples is the use of high resolution TEM (HRTEM) that provides visual as well as analytical data such as size distribution, crystallinity, orientation, defects and interplanar distances on individual nanocrystals. HRTEM micrographs and corresponding selected area electron diffraction (SAED) patterns of single SiN_y:Ge with thickness of around 200 nm before and after annealing using the conventional furnace annealing (CFA) method are shown in figure 5. The sample was annealed at 900 °C for 30 min. It can easily be seen that Ge NCs with well-defined spherical shape are formed. Smaller NCs are obtained for samples annealed for shorter times. The sizes of NCs were determined from TEM micrographs. The size distribution and average sizes of SiN_y:Ge nanocrystals were estimated to vary in the range of 2.8–7.0 nm, in samples annealed under different conditions.

Figure 5(c) shows Raman spectra of SiN_y:Ge samples annealed for different times and temperatures ranging from 15–60 min and from 850 to 900 °C. These conditions result in the above mentioned sizes. Asymmetric broadening of the Raman line is due to phonon confinement [23]. Phonon confinement also predicts a redshift for a Raman peak relative to the bulk Ge peak at 300.7 cm^{-1} [23]. However, instead of the redshift, the Raman line is blueshifted in the samples. The blueshift arises from external compressive stress on the nanocrystal induced by the surrounding matrix. The origin of the compressive stresses observed here and in other reports [23–25] for Ge nanocrystals embedded in a dielectric matrix has not been conclusively, established. The difference in thermal expansion coefficients of Ge and the matrix is expected to lead to tensile strain instead of compressive strain and, therefore, cannot be responsible for the observed compressive stress.

It has been proposed that Ge nanocrystals nucleate and grow in the liquid phase and, due to volume expansion of Ge during solidification, the matrix exerts a compressive stress on the solid nanocrystal [23]. As a result of this compressive stress, masking the redshift originating from confinement of

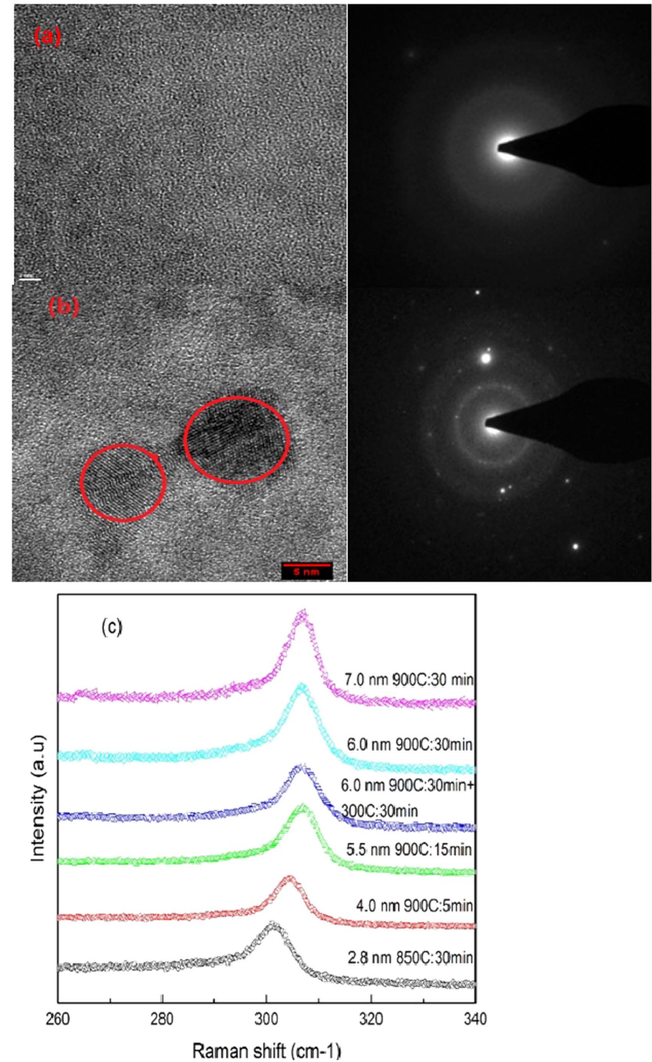

Figure 5. Typical HRTEM micrographs and SAED patterns of a200 nm thick single layer (SiN:Ge150) SiN_y:Ge sample (a) before and (b) after annealing at 900 °C for 30 min in a conventional furnace. No sign of crystallization is seen in the micrograph of the as-grown samples. Transformation from the amorphous phase to nanocrystalline is clearly seen. (c) The Raman spectrum of SiN_y:Ge samples annealed under different conditions using conventional furnace annealing. Average nanocrystal sizes as determined from HRTEM micrographs are also shown corresponding to each spectrum.

phonons in nanocrystals, the Raman peak generally has a blueshift. This Raman shift can be presented as:

$$\Delta\omega_{TO} = \Delta\omega_{strain} + \Delta\omega_{PCM}. \quad (1)$$

To distinguish stress induced shift from phonon confinement induced shift, the phonon confinement model proposed in [26] can be used to calculate the contribution of phonon confinement induced shift. By comparing the calculated shift with the observed experimental shift, one can extract stress induced shift. Instead of a propagating phonon that decays with an arbitrary parameter, α, in the standard phonon confinement model, the said model, proposed by Meilakhs and Koniakhin, takes into account the fact that in a nanocrystal smaller than the phonon mean free path, confined

phonons reflect and scatter at the nanoparticle boundaries during the lifetime of the phonon, leading to a standing wave. Using a finite chain model, they show that redshift of the maximum, bulk frequencies are due to the finite range of phonon wavevectors. Assuming rectangular parallelpiped shaped cubic nanocrystals such as Si and Ge and using dispersion for optical phonons as:

$$\omega(q) = A + B\cos(qa) \quad (2)$$

they show that the frequency shift for of the optical phonons in a nanocrystal due to phonon confinement is given as [26]:

$$\Delta\omega = -(3\pi^2 a^2 B/2(L + a)^2). \quad (3)$$

Here, $B = 18.6\ \mathrm{cm}^{-1}$, '$a$' is the bulk Ge lattice constant and L is the NC diameter. Further details of the method are presented in our previous work [27]. Our results show that, for single layers, stress induced shift is independent of the nanocrystal size and is around $8.1 \pm 0.2\ \mathrm{cm}^{-1}$ for all nanocrystal sizes. The dependence of Raman frequency for the optical phonon, $\omega_{\mathrm{TO},}$ on pressure in bulk Ge has previously been given as [28]:

$$\omega_{\mathrm{TO}} = 300.7 + 3{,}85\ P - 0.039\ P^2 \quad (4)$$

where 'P' is the pressure in GPa and ω_{TO} is the optical phonon frequency in cm^{-1}. Therefore, the pressure on the NCs would be 2.2 ± 0.1 GPa. In order to observe the effects of rapid temperature rise in these samples, we also used RTP for crystallization of Ge in N_2 ambient. Figure 6 shows HRTEM images of sample RTP annealed at 900 °C for 90 s.

As can be seen from TEM micrographs, a conventional furnace annealed sample displays relatively larger NCs compared to RTP annealed ones at the same annealing temperature. This is due to the much longer annealing duration of furnace annealing, which assists the diffusion of Ge atoms and therefore the growth of the NCs.

Raman spectra of the RTP annealed samples are shown in figure 6(c). In all samples, blueshift of the Raman peak relative to bulk Ge is observed, indicating the presence of compressive stress. Relatively smaller blueshifts between samples reflect small variation in size with annealing temperature. Strong compressive stress observed in RTP annealed samples are similar to furnace annealed samples. We found the stress induced shift for RTP samples to be around $8.7\ \mathrm{cm}^{-1}$, which is slightly larger than CFA samples. This might be due to the faster process of solidification in RTP samples. A few reports [3, 4] have discussed that conventional furnace annealing leads to higher activation energy for nucleation and therefore slower crystallization when compared with RTP processed samples. This assists Ge nanocrystals to form facets so as to minimize the interfacial energy. In the process of faceting, it is energetically favorable for the NCs to grow along planes that exert the least pressure on the matrix, as it enables them to minimize their strain energy and thus minimize stress for the NCs. In summary, RTP samples show smaller NCs and slightly higher compressive stress compared to CFA samples.

Despite their widespread use in the microelectronics industry there are significant optical, electrical and structural differences between different dielectrics. Most notably, the industry standards SiO_x and SiN_y behave differently in many respects. For example, the high diffusivity of Ge in SiO_x when compared with its diffusivity in SiN_y plays a significant role in NC formation [11, 12]. We therefore studied single layers of SiO_x:Ge with HRTEM and Raman spectroscopy to compare the results we obtained from SiN_y:Ge layers. The Ge content of samples here is around 24%, which was determined by XPS (XPS results not shown here). In figure 7, we present HRTEM micrographs of the SiO_x:Ge layer annealed at 900 C for 30 min in a conventional furnace. We observe well-formed hexagonal and spherical shape nanocrystals, with hexagonal shaped ones showing facets of the nanocrystals that are bounded by crystal planes. This implies that it is possible to obtain NCs where the equilibrium interface energy is a minimum at 900 °C for Ge NCs in the silicon oxide matrix. Growing NCs in parallel to crystal planes might reduce the pressure on the NC and therefore lower the compressive stress.

We also measured the stress state of Ge NCs in a silicon oxide matrix. Figure 7(c) shows the Raman spectra of the Ge:SiO_x samples. It is observed that crystallization starts at a relatively lower temperature (825 °C) for Ge NCs in a silicon oxide matrix compared to ones embedded in silicon nitride whose threshold crystallization is at 850 °C. This is suggested to be due to the higher diffusivity of Ge atoms in a silicon oxide matrix, which leads to earlier crystallization. Stress analysis is done taking into account phonon confinement induced shift and stress induced shift. The same analysis for NCs embedded in silicon nitride shows a smaller compressive stress for NCs in silicon oxide matrix. Our stress analysis shows the compressive stress for the NCs to be $1.2 \pm 0.2\ \mathrm{cm}^{-1}$. Figure 8 summarizes the stress state of Ge NCs embedded in silicon nitride and silicon oxide matrices.

The stress of NCs has different values in silicon oxide and silicon nitride matrices, and is in the compressive stress form. Ge NCs in a silicon oxide matrix represent smaller compressive stress compared to those embedded in a silicon nitride matrix. This could be due to different lattice constants in a silicon oxide and silicon nitride matrices, which leads to different states of mismatch between nanocrystals and the surrounding matrix and therefore the stress state. NCs in the silicon oxide matrix are also formed at relatively lower annealing temperature, which in turn leads to less thermal stress. Also due to more diffusivity of the Ge NCs in the silicon oxide matrix and easier formation of NCs in terms of energy considerations, NCs form in the equilibrium state with planes parallel to crystal facets, which in turn leads to decreasing the pressure on the NC. However, for NCs in any matrix, this stress is independent of NC size in the range studied. This is in agreement with the work of [23] who reported similar stress values for small NCs. They argued that below a given size, pressure is saturated and, therefore, a constant stress value exists for small enough particles.

Our results show crystallization of Ge NCs in oxide and nitride matrices is associated with compressive stress. The stress state of NCs in each matrix is constant and does not depend on the size of the NCs, however different values of

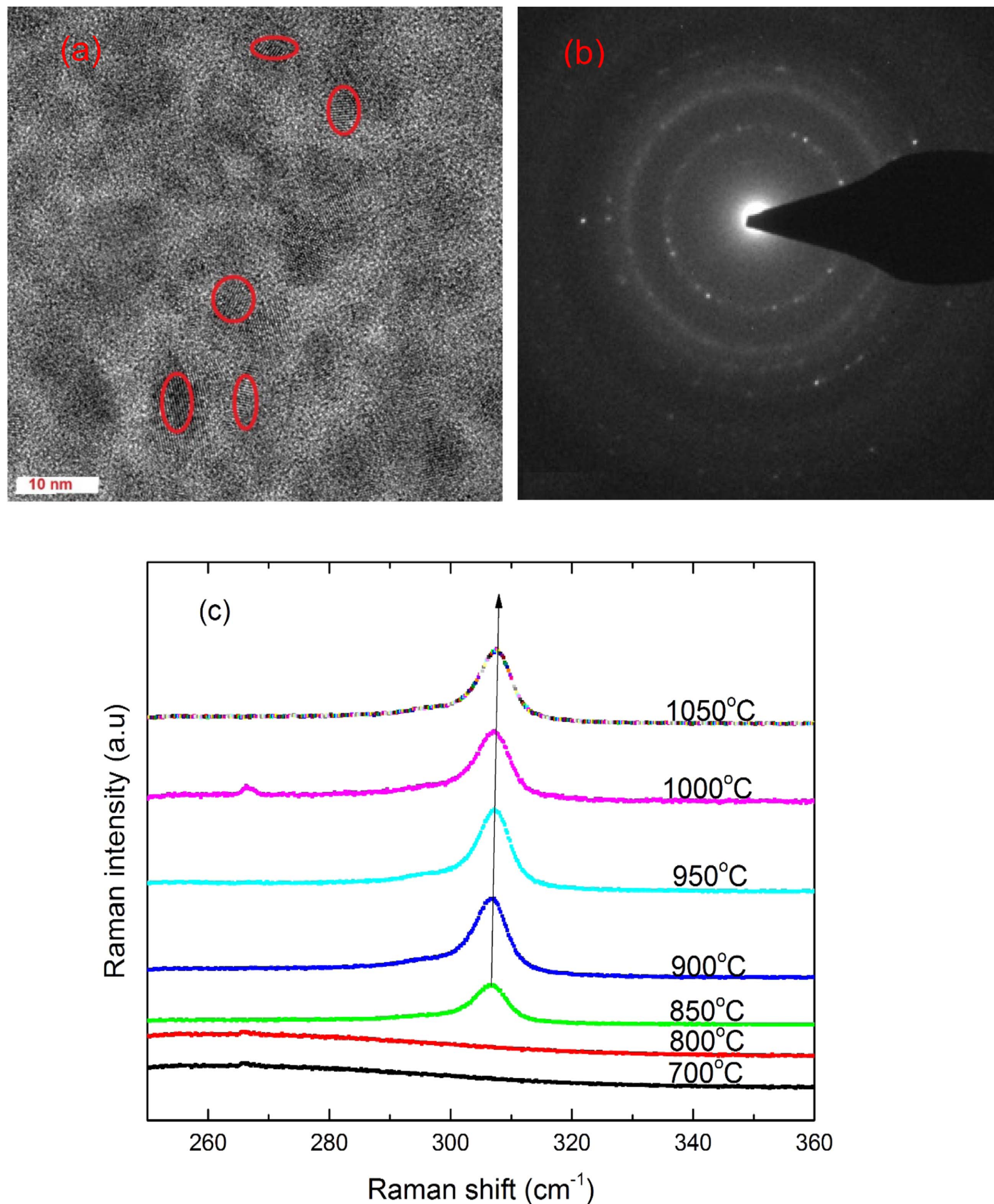

Figure 6. (a) The HRTEM micrograph and (b) the SAED pattern of the RTP annealed sample (sample SiN:Ge150). Smaller NCs are formed during RTP annealing compared to samples annealed in a conventional furnace. (c) Raman spectra of SiN_y:Ge samples annealed at different temperatures with RTP for 60 s. In all samples, blueshift of the Raman peak compared to bulk Ge is observed, indicating the presence of compressive stress. Relatively smaller blueshifts between samples reflect small variation in size with annealing temperature.

stress present in oxide and nitride embedded NCs with larger compressive stress for Ge NCs in silicon nitride matrix.

Stress evolution of Ge NCs in superlattices with buffer layers

We also synthesized Ge NCs in superlattice samples. Here ultrathin Ge:SiN_y films are separated with stoichiometric SiO_2 or Si_3N_4 thin films. This closely spaced Ge NC structure would be potentially advantageous for third generation solar cells as this structure could improve electrical conductivity while confining the NC growth. This approach also allows for controlling simultaneously the size and density of NCs. Here, we fabricated two different sets of superlattices: SiN_y:Ge/SiO_2 and SiN_y:Ge/Si_3N_4, and use HRTEM and Raman study to investigate the stress state in samples. Figure 9 shows depth profile XPS measurements on the multilayer 6 nm thick SiN_y:Ge in the 25 nm SiO_2 buffer layer sample. For clarity, only the first 20 etch cycles are included in the figure. As seen from the figure, no Ge $2p_{3/2}$ signal was detected for the first six etch cycles. This implies the first 25 nm top SiO_2 buffer layer. The Ge $2p_{3/2}$ line was observed between the 7th and 11th cycles, which corresponds to the first SiN_y:Ge NC layer from the top. The second SiO_2 buffer layer and the Ge $2p_{3/2}$ line can also be seen from the figure between 12 and 15, and 16 and 20 etch cycles, respectively. Clear separation of the buffer layer and the SiN_y:Ge NC layer confirms no diffusion of the Ge into the SiO_2 buffer layer. Furthermore, observation of slow strengthening of the Ge

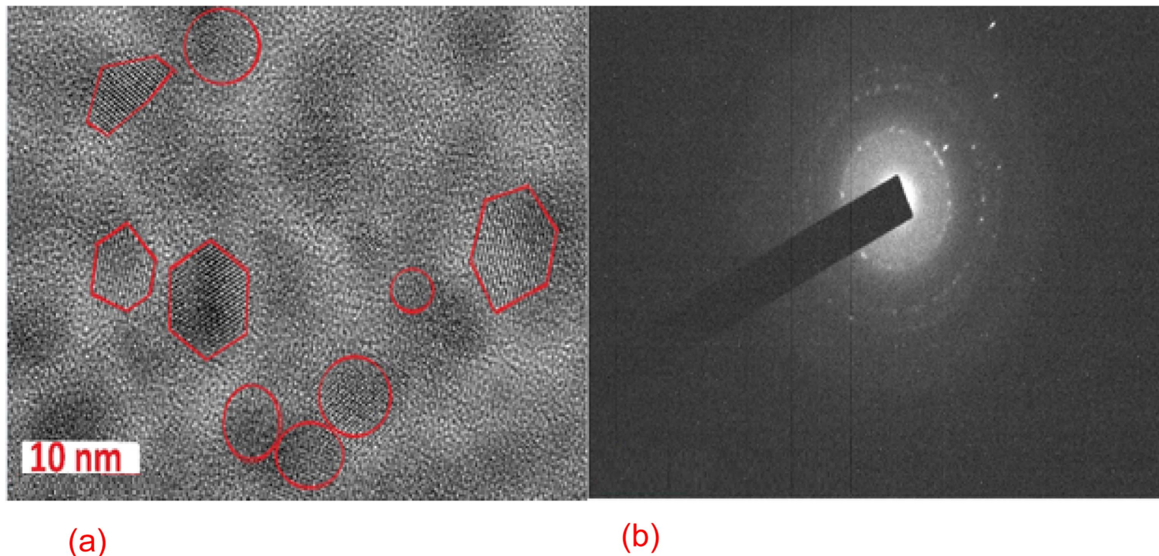

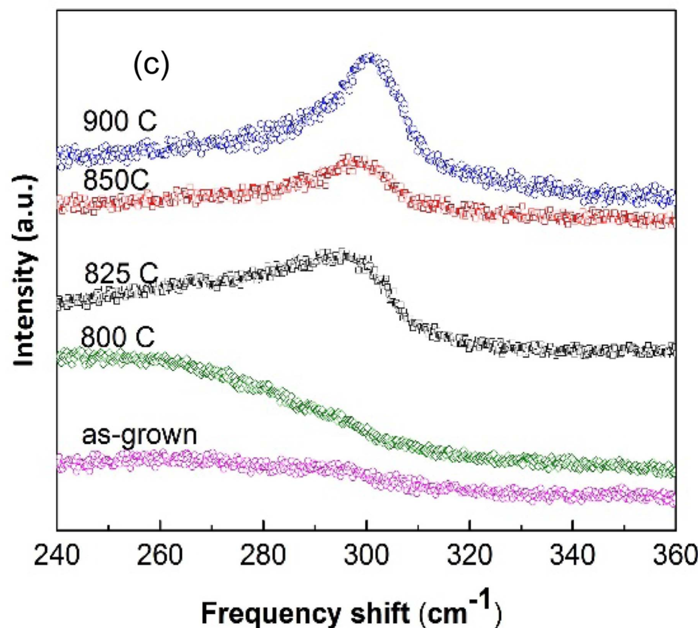

Figure 7. (a) HRTEM micrographs and (b) associated SAED) pattern for SiO_x:Ge annealed at 900 °C for 30 min. The faceted shape of the NCs implies that it is possible to obtain the equilibrium interface energy minimizing configuration at 900 °C for NCs in silicon oxide. (c) Raman spectra of Ge NCs embedded in a silicon oxide matrix annealed at different temperatures. Note the shoulder springing up at 825 C where NC formation starts.

$2p_{3/2}$ peak intensities and then annihilation of the peak depicts the same behavior. These show the suitability of the SiO_2 as the buffer layer due to suppressing the diffusion of Ge. However, the binding energy of the Ge $2p_{3/2}$ lines shifts to the lower energy values as the number of etch cycles increases. The total shift observed is 0.6 eV towards elemental values of Ge $2p_{3/2}$. We suggest that the shift is due to observation of more elemental Ge as the beam reaches deeper into the sample. The higher energy gives rise to the formation of the oxidation chemical states of Ge, GeO and/or GeO_2. Apparently, the top layers of the SiN_y:Ge NC involve oxidized states of Ge, while the layers formed close to the substrate include more elemental Ge. The oxidation of the top layers likely takes places during annealing.

In figure 10(a), we show HRTEM micrographs of multilayers consisting of ultrathin SiN_y:Ge films and stoichiometric SiO_2 buffer layers, which are used as buffers for Ge diffusion and controlling the size of the NCs. The thickness of SiN_y:Ge and SiO_2 buffer layers are the same in a given sample. However, the thickness of the SiN_y:Ge layer is varied between 3.0 to 9.0 nm from sample to sample. The undulations in the Ge containing layer shows that there is some Ge diffusion into the buffer layers, as Ge diffuses in plane during crystallization. It is noteworthy that the undulation amplitude increases in the Ge containing layers away from the substrate. In the extreme case, we may expect that undulations lead to spherical droplets in the form of worry beads in order to minimize the total energy of formation. Figure 10(b) indicates

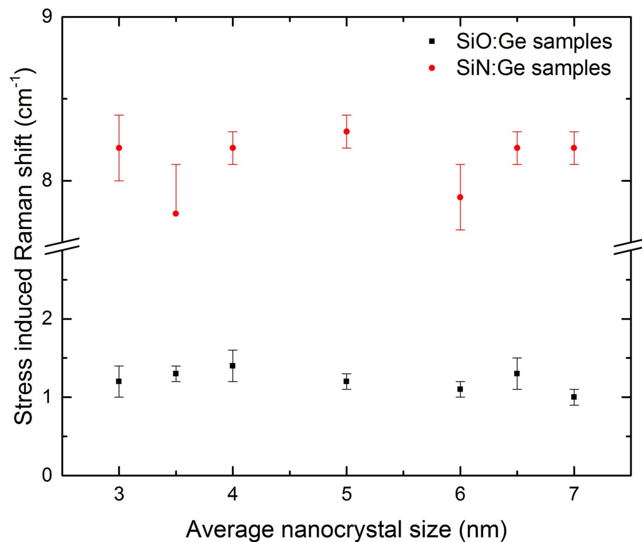

Figure 8. Strain in Ge NCs in single layer silicon nitride and silicon oxide matrices as measured by Raman shift deconvoluted for the phonon confinement effect calculated for sizes as measured from HRTEM data.

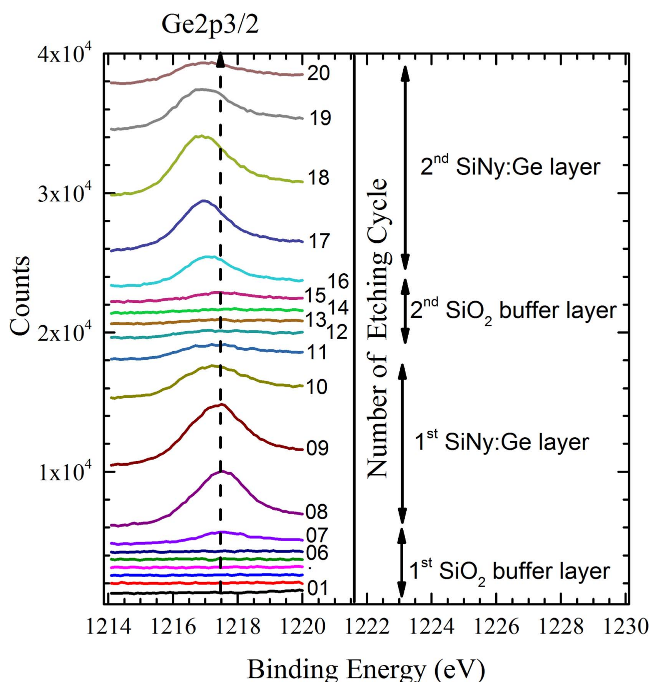

Figure 9. Depth XPS of multilayer 6 nm thick SiN_y:Ge in the 25 nm SiO_2 buffer layer sample. For clarity only the first 20 etch cycles are included in the figure. The dashed line references the Ge $2p_{3/2}$ peaks closer to the surface. Deeper Ge $2p_{3/2}$ peaks shift towards the elemental Ge $2p_{3/2}$ line.

that annealing at 900 °C leads to Ge diffusion to form a mixture of amorphous and nanocrystal clusters. We would expect that at longer anneal durations or higher temperatures all material would be crystalline in the form of undulated nanosheets.

Figure 11 shows the Raman spectrum of multilayer SiGeN:SiO_2 samples annealed at different temperatures. Compressive stress is observed for all samples. Stress induced Raman shift is calculated taking into account a simple phonon confinement model [26]. Table 2 summarizes the correlation between stress, size and crystallization threshold for SiN_y:Ge/SiO_2 samples. As can be seen, smaller NCs experience larger compressive stress. The temperature thresholds for crystallization for samples with thicknesses 3, 6 and 9 nm are 775 °C, 800 °C and 850 °C, respectively. This can be discussed in terms of different values of stress for different samples. As we see there is a rather strong correlation between the crystallization threshold and compressive stress in these multilayer samples. We observe that the more compressive stress there is, the lower the temperature threshold for crystallization.

The spectra for 3 nm thick SiN_y:Ge layers are detailed and illustrative. On annealing at 775 °C, a shoulder starts to develop at around 300 cm^{-1}. At higher temperatures this shoulder develops into a fully fledged peak and shifts towards the red.

For sample with 3.0 nm SiN_y:Ge, stress induced Raman shift is 9.4 cm^{-1} with the corresponding crystallization temperature threshold being 775 °C. For samples with Ge nanocrystal sizes of 6.0 nm and 8.4 nm, stress induced Raman shift is 4.9 cm^{-1} and 2.1 cm^{-1}, respectively. We note that in contrast to single layer samples, stress on nanocrystals is size dependent in multilayer samples with larger stress for smaller nanocrystals. Notice that in multilayer samples, the environment of the nanocrystal is more complicated, where they are partially surrounded by silicon nitride and also by buffer layers and the therefore stress relation on NCs can be complex. Further work is needed to study the details of stress accumulation in this type of sample. For these samples, the crystallization temperature threshold is between 800 °C and 850 °C. This is in agreement with work in [29]. In that work, it was shown that application of an external mechanical compressive stress during annealing for copper-induced growth of polycrystalline Ge leads to enhancement of crystallization.

We also analyzed multilayers with near stoichiometric Si_3N_4 as buffer layers: SiN_y:Ge/Si_3N_4 multilayers. For SiN_y:Ge/Si_3N_4 samples that experience tensile strain the crystallization threshold is 950 °C. This is in agreement with several reports [30, 31] for the observed role of stress in crystallization of Si and SiGe. It has been reported that the annealed PECVD SiN_y films exhibit considerable tensile strain. This tensile strain increases with annealing temperature from 750 °C and saturates at a value of 1.2 GPa at around 1100 °C [32, 33]. This is suggested to be linked to the release of hydrogen and reformation of the Si–N bond network after the annealing. SiN_y is commonly used as a buffer material to prevent interdiffusion of metal and semiconductor. Therefore, it is reasonable to expect that, in the sample with the SiN_y cap, the relatively higher Ge supersaturation would lead to a reduction of buffer to nucleation and hence faster NC formation.

Figures 12(a) and (b) illustrate TEM micrographs of multilayer samples with Si_3N_4 buffer layers annealed at 900 °C for 30 min. Crystallization starts at the layer next to the substrate. NCs are observed for other layers in the sample

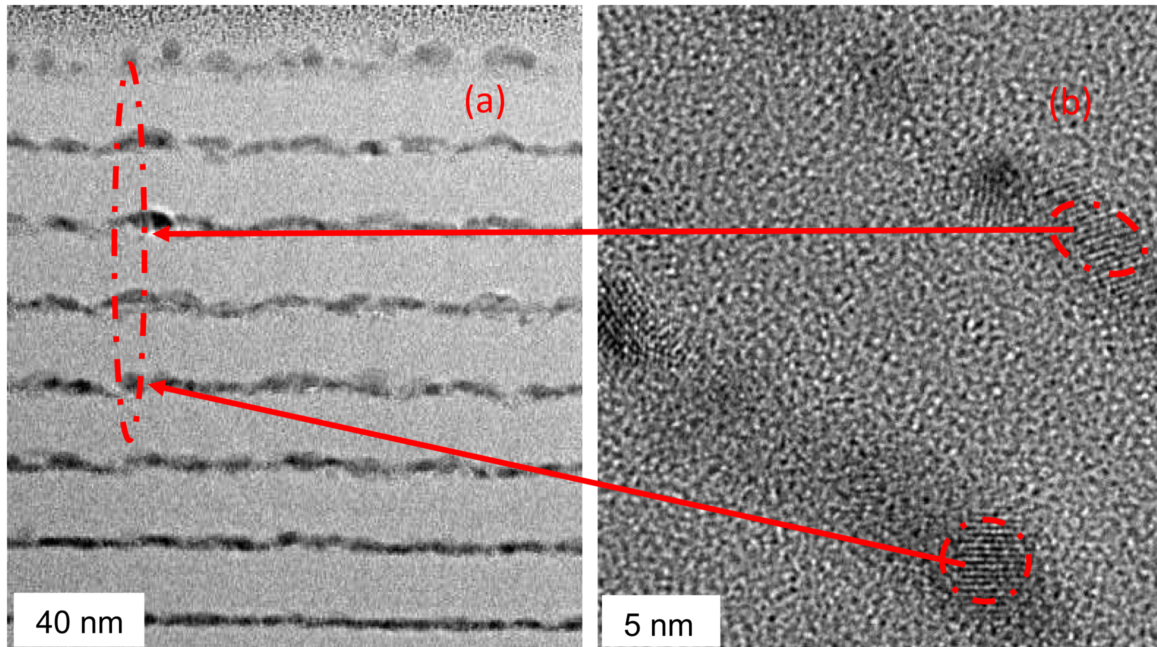

Figure 10. TEM micrographs of multilayer SiN_y:Ge samples with SiO_2 buffer layers. The thickness of SiN_x:Ge and SiO_2 buffer layers are the same in a given sample. However, the thickness of the SiN_y layer is varied between 3.0 to 9.0 nm from sample to sample. The undulations in the Ge containing layer shows that there is some Ge diffusion into the buffer layers, as Ge diffuses in plane during crystallization.

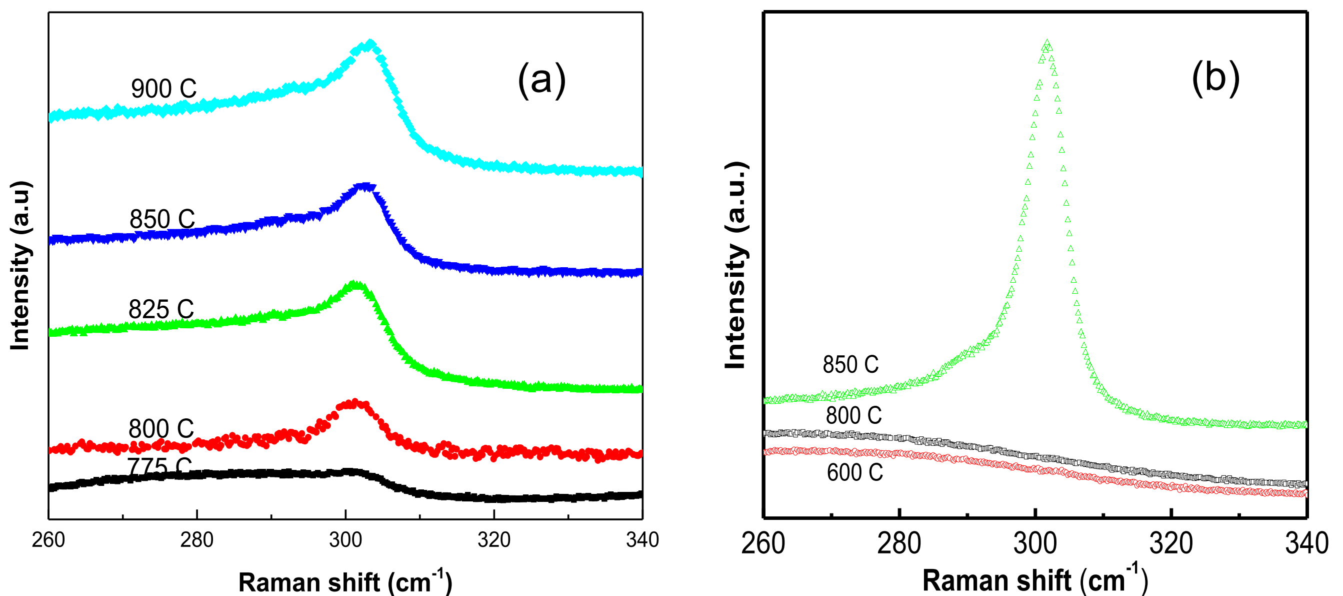

Figure 11. Raman spectra for (a) 3 nm and (b) 9 nm thick SiN_y:Ge samples separated by Si_3N_4 buffer layers annealed at various temperatures. We compare the threshold crystallization temperature for 3 nm thick samples at 775 °C with those for 9 nm thick samples at ∼825 °C.

Table 2. Stress induced frequency shift and correlation between stress and crystallization threshold for SiN_y:Ge/SiO_2 multilayers.

Sample ID	Average size (nm)	Total Raman shift (cm^{-1})	Stress induced Raman shift (cm^{-1})	Crystallization threshold
ML3	3.0	2.4	9.4	775 °C
ML6	6.0	2.7	4.9	800 °C
ML9	8.5	1.0	2.1	850 °C

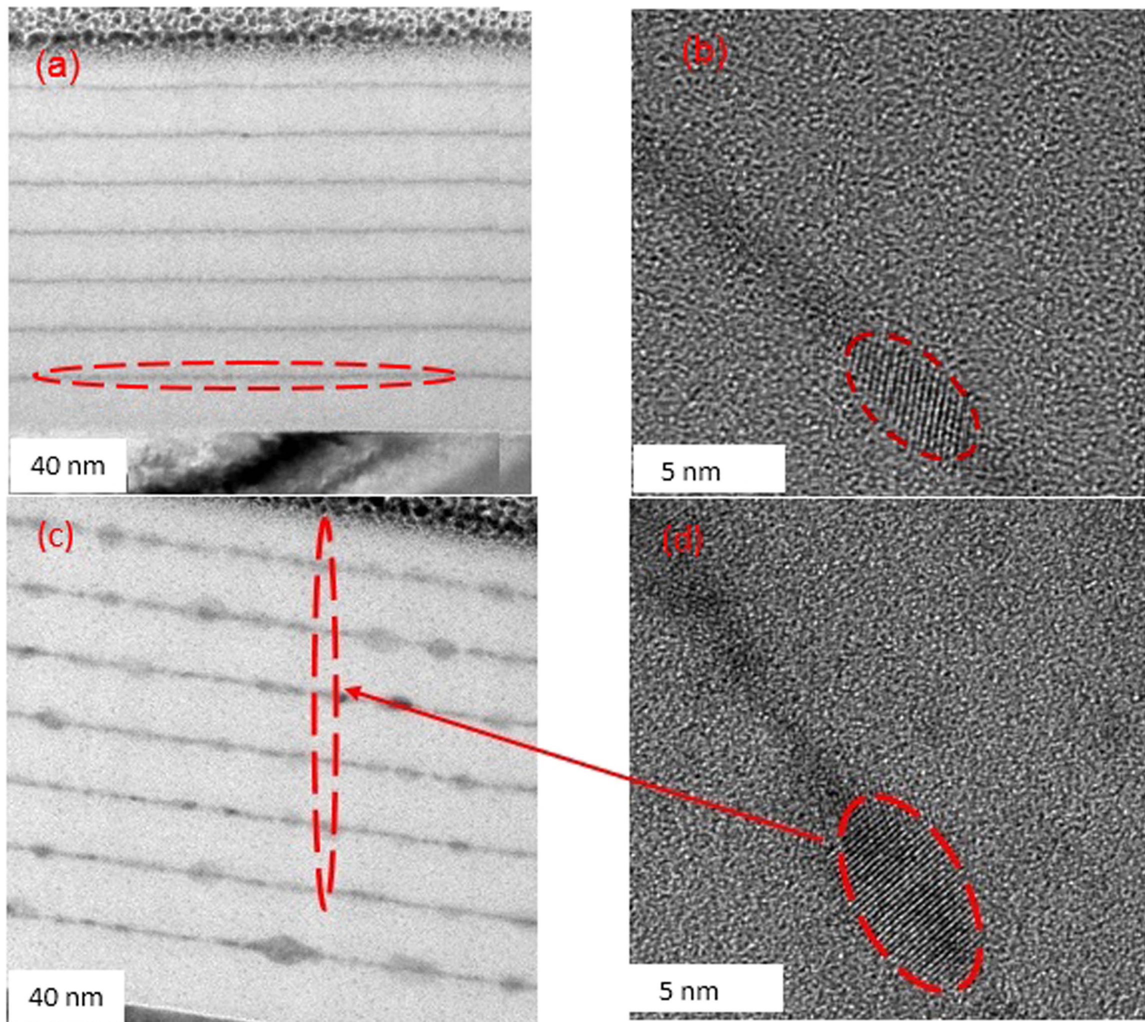

Figure 12. (a) and (b) Cross-sectional TEM micrograph of SiN_y:Ge/Si_3N_4 multilayers annealed at 900 °C for 30 min. The dark lines correspond to SiN_y:Ge layers and the white bands to Si_3N_4 buffer layers. NCs are formed only in the layer next to the substrate. (c) and (d) The same sample after annealing at 1000 °C for 30 min. NCs are formed in all layers with larger sizes compared to the sample annealed at 900 °C.

annealed at 900 °C. This is suggested to be due to the existence of higher nucleation energy at layers closer to the substrate. Consequently, Ge nanocrystals can nucleate and form earlier and faster. Figures 12(c) and (d) show HRTEM of the sample after annealing at 1000 °C for 30 min. At this temperature NCs are formed in all layers due to the higher activation energy at this temperature. Moreover, the size of the NCs is larger compared to the sample annealed at 900 °C. This agrees well with the Raman spectra shown in figure 13 where we again used formula (3) for PCE induced Raman shift [30].

In figure 13, Raman spectra of multilayer samples consisting of Si_3N_4 ultrathin films as buffer layers are shown. The sample annealed at 900 °C shows no Raman peak, which is in agreement with results obtained via HRTEM micrographs. The threshold for crystallization for these multilayer structures is around 950 °C. Moreover, despite single layer samples and multilayer samples with SiO_2 as buffer there is a large redshift in the Raman peak, which is because of tensile strain presents in the samples. Table 3 summarizes the

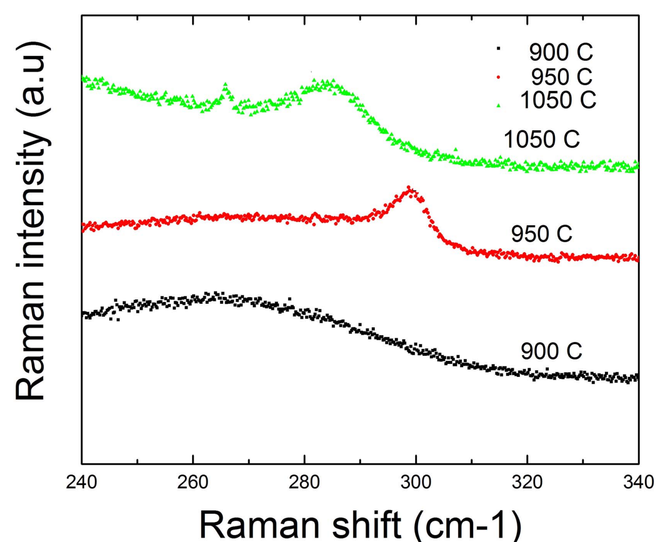

Figure 13. Raman spectra of SiGeN/Si_3N_4 multilayer samples. The large redshift of the Raman peak illustrates the presence of tensile stress.

Table 3. Stress induced shift and correlation between stress and crystallization threshold for SiN_y:Ge/Si_3N_4 multilayers.

Sample ID	Average nanocrystal size (nm)	Total Raman shift (cm^{-1})	Stress induced Raman shift (cm^{-1})	Crystallization threshold
ML6	6.3	−16.2	−14.0	950 °C
ML4	4.4	−4.7	−1.2	950 °C

correlation between crystallization temperature threshold and tensile strain. The samples are labeled as ML4 and ML6 with the numbers showing the approximate size of the NCs, which are around 4 and 6 nm respectively. Sample ML4 was annealed at 950 °C for 30 min while ML6 was annealed at 1050 °C for 60 min, which led to the formation of larger NCs. Both samples represent considerable redshift. Sample ML4 shows a tensile strain of $-1.2\,cm^{-1}$, while increasing annealing time and temperature leads to more redshift, reaching to a tensile strain of $-14.4\,cm^{-1}$ for sample ML6 annealed at 1050 °C for 60 min. This corresponds to a tensile stress of 3.8 GPa obtained from equation (2). At temperatures as high as 1050 °C, Ge becomes molten and its diffusivity increases drastically, therefore larger NCs are formed. Note also that when annealed at 1050 °C, the viscosity of the silicon oxide decreases and this will also assist in the stress relief for the NCs. This can lead to the reduction of intrinsic compressive stress present in the NCs or, in other words, more redshift in the Raman peak. We suggest that most notable is the strain associated between the buffer and layer in question.

Figure 14 shows correlation between the crystallization threshold temperature and stress on germanium nanocrystals for multilayer samples. For the sample experiencing largest compressive stress, crystallization starts at around 775 °C, however for the sample with tensile stress this temperature is 1000 °C. This is in agreement with works of several groups who reported the relation between stress and crystallization [29, 34, 35]. As tensile strain increases, the strain energy at the Ge NC surface increases, and the Ge–Ge bonds become more stretched at the surface of the Ge NC. When the strain energy eventually becomes comparable to the bond energy of the Ge atoms, the Ge atoms will preferentially detach from the surface of the NC, which slows the growth of the NCs. As a result, for tensile strained samples higher temperatures are required to provide high kinetic energy for Ge atoms to be involved in the crystallization process. Crystallization at lower temperatures is a desirable property in technological applications. Lowering the crystallization temperature by controlling stress can be a useful approach that leads to decreased processing thermal budget.

Kimura *et al* [36] investigated the effect of stress on a-Si and observed suppression of crystallization by applying tensile strain. A compressive stress-assisted, Cu induced lateral-crystallization technique for the preparation of polycrystalline Ge at temperatures as low as 150° C has also been [29] reported. Huang *et al* [31] also reported the positive effect of compressive stress on crystallization of a-Si. However, some reports have shown that tensile strain assists the crystallization. Recently, the effects of external mechanical stress on

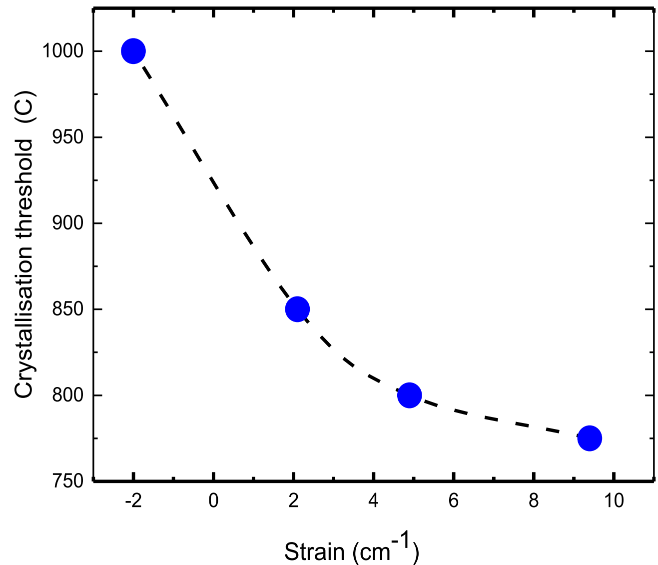

Figure 14. Threshold temperature for crystallization of Ge NCs as a function of strain as measured by Raman shift of the Ge TO line.

the crystallization of amorphous silicon have been reported by Hashemi *et al* [37]. It was shown that tensile stress applied to silicon films during annealing enhanced the crystallization properties of silicon, while an applied compressive stress suppresses the crystallization process.

Our results show the enhancement of crystallization when under compressive stress and reduced crystallization in tensile strained samples. Kimura [38] used a model to discuss the effect of stress on crystallization of a-Si. Based on this model the driving energy of crystallization is the difference in Helmholtz energy between c-Si and a-Si under stress. According to this analysis when the stress does not relax the driving energy decreases which leads to reduction in crystallization and therefore crystallization starts at higher temperatures. The effect of compressive and tensile strain on crystallization needs to be further investigated.

Conclusions

Fabrication of germanium NCs in a dielectric matrix leads to a residual stress that is usually in the form of compressive stress. In the present work, we aimed to change the stress state of the NCs from the intrinsic compressive state to tensile stress by changing the annealing conditions, the dielectric matrix material or the buffer as a stressor. We fabricated germanium NCs in silicon oxide and silicon nitride matrices

via the PECVD method and post annealing in N_2 ambient. Crystallization was observed via TEM and Raman spectroscopy. The Raman shift of NCs compared to bulk material is mainly due to stress exerted on NCs and confinement of phonons in the nanostructure. We distinguished these two compartments by applying a phonon confinement model to obtain the stress state of the NCs. We found that a constant value of stress exists for NCs in each dielectric matrix. However, the NCs experience different amounts of stress in any matrix, that is changing the matrix does not tune the stress state from compressive to tensile stress but the value of compressive stress. We also examined the effect of annealing method on the stress state of the samples and found small changes in the stress amount of NCs. Finally, we synthesized germanium NCs in superlattice multilayer structures. Two sets of multilayers were fabricated; the first set consisted of SiGeN ultrathin films sandwiched between stoichiometric SiO_2 thin layers, in the second set SiO_2 layers were replaced by stoichiometric Si_3N_4 thin films. For the first set of multilayers with SiO_2 barriers, Ge NCs experience compressive stress, which is size dependent, with larger stress for smaller NCs. For the second set of NCs with Si_3N_4 barriers, tensile stress existed, therefore we were able to tune the stress state of NCs from compressive to tensile via stressor barriers. This is very important as the stress state of Ge is intimately connected to the band gap of the material.

Acknowledgments

The authors acknowledge use of the services and facilities of UNAM-National Nanotechnology Research Center at Bilkent University.

ORCID iDs

Rahim Bahariqushchi

https://orcid.org/0000-0002-3607-9561

References

[1] Gao F, Green M A, Conibeer G, Cho E C, Huang Y, Pere-Wurfl I and Flynn C 2008 Fabrication of multilayered Ge nanocrystals by magnetron sputtering and annealing *Nanotechnology* **19** 455611

[2] Shieh J M, Lai Y F, Ni W X, Kuo H C, Fang C Y, Huang J Y and Pan C L 2007 Enhanced photoresponse of a metal-oxide-semiconductor photodetector with silicon nanocrystals embedded in the oxide layer *Appl. Phys. Lett.* **90** 051105

[3] Pavesi L, Dal Negro L, Mazzoleni C, Franzo G and Priolo F 2000 Optical gain in silicon nanocrystals *Nature* **408** 440

[4] Akca I B, Dâna A, Aydinli A and Turan R 2008 Comparison of electron and hole charge-discharge dynamics in germanium nanocrystal flash memories *Appl. Phys. Lett.* **92** 052103

[5] Maeda Y, Tsukamoto N, Yazawa Y, Kanemitsu Y and Masumoto Y 1991 Visible photoluminescence of Ge microcrystals embedded in SiO2 glassy matrices *Appl. Phys. Lett.* **59** 3168–70

[6] Niquet Y M, Allan G, Delerue C and Lannoo M 2000 Quantum confinement in germanium nanocrystals *Appl. Phys. Lett.* **77** 1182–4

[7] Zacharias M and Fauchet P M 1998 Light emission from Ge and GeO_2 nanocrystals *J. Non-Cryst. Solids* **227** 1058–62

[8] Choi W K, Ng V, Ng S P, Thio H H, Shen Z X and Li W S 1999 Raman characterization of germanium nanocrystals in amorphous silicon oxide films synthesized by rapid thermal annealing *J. Appl. Phys.* **86** 1398–403

[9] Buljan M *et al* 2013 Ge quantum dot lattices in Al_2O_3 multilayers *J. Nanopart. Res.* **15** 1485

[10] Lee S, Huang S, Conibeer G and Green M 2013 Lateral growth of Ge nanocrystals in a thin Ge-rich silicon nitride layer *J. Cryst. Growth* **383** 36–42

[11] Mirabella S, Cosentino S, Gentile A, Nicotra G, Piluso N, Mercaldo L V, Simone F, Spinella C and Terrasi A 2012 Matrix role in Ge nanoclusters embedded in Si_3N_4 or SiO_2 *Appl. Phys. Lett.* **101** 011911

[12] Sharp I D *et al* 2005 Mechanism of stress relaxation in Ge nanocrystals embedded in SiO_2 *Appl. Phys. Lett.* **86** 063107

[13] Yuan C, Liu Q and Xu B 2011 Strain-induced structural phase transition of Si nanoparticles *J. Phys. Chem.* C **115** 16374–7

[14] Yuan C, Ye S, Xu B and Lei W 2012 Strain induced tetragonal $SrTiO_3$ nanoparticles at room temperature *Appl. Phys. Lett.* **101** 071909

[15] Liao P H, Hsu T C, Chen K H, Cheng T H, Hsu T M, Wang C C, George T and Li P W 2014 Size-tunable strain engineering in Ge nanocrystals embedded within SiO_2 and Si_3N_4 *Appl. Phys. Lett.* **105** 172106

[16] Ghrib A *et al* 2012 Control of tensile strain in germanium waveguides through silicon nitride layers *Appl. Phys. Lett.* **100** 201104

[17] Ishikawa Y, Wada K, Cannon D D, Liu J, Luan H C and Kimerling L C 2003 Strain-induced band gap shrinkage in Ge grown on Si substrate *Appl. Phys. Lett.* **82** 2044–6

[18] Bai Y, Lee K E, Cheng C, Lee M L and Fitzgerald E A 2008 Growth of highly tensile-strained Ge on relaxed $In_xGa_{1-x}As$ by metal-organic chemical vapor deposition *J. Appl. Phys.* **104** 084518

[19] Fang Y Y, Tolle J, Roucka R, Chizmeshya A V G, Kouvetakis J, D'Costa V R and Menéndez J 2007 Perfectly tetragonal, tensile-strained Ge on $Ge_{1-y}Sn_y$ buffered Si(100) *Appl. Phys. Lett.* **90** 061915

[20] De Kersauson M, El Kurdi M, David S, Checoury X, Fishman G, Sauvage S, Jakomin R, Beaudoin G, Sagnes I and Boucaud P 2011 Optical gain in single tensile-strained germanium photonic wire *Opt. express* **19** 17925–34

[21] Mayer M 1997 SIMNRA User's Guide, Report IPP 9/113 Garchin (Max Planck Institut für Plasmaphysik, 1997)

[22] Bahariqushchi R, Gündoğdu S and Aydinli A 2017 Ge nanocrystals embedded in ultrathin Si_3N_4 multilayers with SiO_2 barriers *Superlatt. Microstruct.* **104** 308–15

[23] Wellner A, Paillard V, Bonafos C, Coffin H, Claverie A, Schmidt B and Heinig K H 2003 Stress measurements of germanium nanocrystals embedded in silicon oxide *J. Appl. Phys.* **94** 5639–42

[24] Cheung A, Azevedo G de M, Glover C.J., Llewellyn D.J., Elliman R.G., Foran G.J. and Ridgway M.C 2004 Structural perturbations within Ge nanocrystals in silica *Appl. Phys. Lett.* **84** 278–80

[25] Kartopu G, Karavanskii V A, Serincan U, Turan R, Hummel R E, Ekinci Y, Gunnæs A and Finstad T G 2005 Can chemically etched germanium or germanium nanocrystals emit visible photoluminescence? *Phys. Status Solidi* (a) **202** 1472–6

[26] Meilakhs A P and Koniakhin S V 2017 New explanation of Raman peak redshift in nanoparticles *Superlatt. Microstruct.* **110** 319–23
[27] Bahariqushchi R, Gündoğdu S and Aydinli A 2017 Correlation of TEM data with confined phonons to determine strain and size of Ge nanocrystals embedded in SixNy matrix *Superlatt. Microstruct.* **111** 90–5
[28] Olego D and Cardona M 1982 Pressure dependence of Raman phonons of Ge and 3C-SiC *Phys. Rev.* B **25** 1151
[29] Hekmatshoar B, Mohajerzadeh S, Shahrjerdi D, Afzali-Kusha A, Robertson M D and Tonita A 2005 Low-temperature copper-induced lateral growth of polycrystalline germanium assisted by external compressive stress *J. Appl. Phys.* **97** 044901
[30] Hekmatshoar B, Shahrjerdi D, Mohajerzadeh S, Khakifirooz A, Robertson M, Tonita A and Bennett J C 2004 Low-temperature stress-assisted germanium-induced crystallization of silicon–germanium alloys on flexible polyethylene terephtalate substrates *J. Vac. Sci. Technol. A* **22** 856–8
[31] Huang S Y, Lin H L, Chao C G and Liu T F 2012 Effect of compressive stress on nickel-induced lateral crystallization of amorphous silicon thin films *Thin Solid Films* **520** 2984–8
[32] Morin P, Martinez E, Wacquant F and Regolini J L 2005 Thermal stress relaxation of plasma enhanced chemical vapour deposition silicon nitride *MRS Online Proc. Library Archive* p 875
[33] Hughey M P and Cook R F 2004 Massive stress changes in plasma-enhanced chemical vapor deposited silicon nitride films on thermal cycling *Thin Solid Films* **460** 7–16
[34] Lee B J, Lee C S and Lee J C 2003 Stress induced crystallization of amorphous materials and mechanical properties of nanocrystalline materials: a molecular dynamics simulation study *Acta Mater.* **51** 6233–40
[35] Park J, Kwon S, Jun S I, Ivanov I N, Cao J, Musfeldt J L and Rack P D 2009 Stress induced crystallization of hydrogenated amorphous silicon *Thin Solid Films* **517** 3222–6
[36] Kimura Y, Kishi M and Katoda T 1999 Effects of elastic stress introduced by a silicon nitride cap on solid-phase crystallization of amorphous silicon *J. Appl. Phys.* **86** 2278–80
[37] Hashemi P, Derakhshandeh J, Mohajerzadeh S, Robertson M and Tonita A 2004 Stress-assisted nickel-induced crystallization of silicon on glass *J. Vac. Sci. Technol. A* **22** 966–70
[38] Kimura Y, Kishi M and Katoda T 2000 The model of solid phase crystallization of amorphous silicon under elastic stress *J. Appl. Phys.* **87** 4017–21